GEOPHYSICAL RESEARCH LETTERS, VOL. 36, L23204, doi:10.1029/2009GL041234, 2009

Dielectric properties of lava flows west of Ascraeus Mons, Mars

Lynn M. Carter,[1] Bruce A. Campbell,[1] John W. Holt,[2] Roger J. Phillips,[3] Nathaniel E. Putzig,[3] Stefania Mattei,[4] Roberto Seu,[5] Chris H. Okubo,[6] and Anthony F. Egan[3]

Received 5 October 2009; revised 5 November 2009; accepted 12 November 2009; published 12 December 2009.

[1] The SHARAD instrument on the Mars Reconnaissance Orbiter detects subsurface interfaces beneath lava flow fields northwest of Ascraeus Mons. The interfaces occur in two locations; a northern flow that originates south of Alba Patera, and a southern flow that originates at the rift zone between Ascraeus and Pavonis Montes. The northern flow has permittivity values, estimated from the time delay of echoes from the basal interface, between 6.2 and 17.3, with an average of 12.2. The southern flow has permittivity values of 7.0 to 14.0, with an average of 9.8. The average permittivity values for the northern and southern flows imply densities of 3.7 and 3.4 g cm^{-3}, respectively. Loss tangent values for both flows range from 0.01 to 0.03. The measured bulk permittivity and loss tangent values are consistent with those of terrestrial and lunar basalts, and represent the first measurement of these properties for dense rock on Mars. **Citation:** Carter, L. M., B. A. Campbell, J. W. Holt, R. J. Phillips, N. E. Putzig, S. Mattei, R. Seu, C. H. Okubo, and A. F. Egan (2009), Dielectric properties of lava flows west of Ascraeus Mons, Mars, *Geophys. Res. Lett.*, *36*, L23204, doi:10.1029/2009GL041234.

1. Introduction

[2] Radar measurements of dielectric properties can provide valuable information on the composition and density of planetary surface materials, and such information could be important to understanding the range of volcanic deposits on Mars. Prior measurements of the dielectric properties of the Medusae Fossae Formation, a possible pyroclastic deposit, have yielded low values (3–4) for the permittivity and low values for the loss tangent (0.001–0.005) [*Watters et al.*, 2007; *Carter et al.*, 2009]. The SHARAD (Shallow Radar) instrument on MRO (Mars Reconnaissance Orbiter) sounded through thin Amazonis Planitia plains materials and the Vastitas Borealis Formation, and the measured loss tangents of 0.005–0.012 are consistent with moderate-density sediments [*Campbell et al.*, 2008]. Bistatic experiments between the orbiting Mars Express spacecraft and the NASA Goldstone antennas at a wavelength of 3.6 cm yielded permittivity values between 2 and 4 across a variety of Martian terrains including the poles and northern plains [*Simpson et al.*, 2007]. Using Arecibo Observatory as a receiver at 13 cm wavelength resulted in permittivity estimates that were 10–50% higher than the 3.6 cm wavelength data across the same terrains [*Simpson et al.*, 2007], consistent with an increase in dust compaction or a transition to dense bedrock in the upper 1 m of the Martian surface. If basaltic lava flows cover considerable areas of Mars, one might expect to see higher measured permittivity values. On Earth, dense (i.e., low vesicularity) basalts have real permittivities between 7 and 11 [*Ulaby et al.*, 1988; *Campbell and Ulrichs*, 1969]. The Martian dust cover, sediments, or weathering products likely blanket many surfaces and obfuscate dielectric measurements at short radar wavelengths. However, radar images at 13 cm wavelength do show large areas of bright flows in the Tharsis, Elysium and Amazonis regions [*Harmon and Nolan*, 2007; *Harmon et al.*, 1999], which are likely indicative of rugged, dense (high-permittivity) lavas. While an exposed high-permittivity surface will permit less penetration by a probing long-wavelength radar wave, a modest covering of dust can greatly reduce this impedance mismatch with the atmosphere and allow for increased penetration.

[3] SHARAD is well suited to determining the dielectric properties of lava flows, provided that it can detect a subsurface interface. If the radar wave penetrates a lava flow and reflects from a basal interface with material of sufficient dielectric contrast, it is possible to calculate the permittivity and loss tangent, given an independent measurement of the flow thickness. The large flow field north and west of Ascraeus Mons is one of the few areas on Mars where the SHARAD radar appears to penetrate dense volcanic rock. In this case a flat, smooth, dust-covered surface provides ideal conditions for measuring the material properties of these flows. The values reported here represent the first measurements of the dielectric properties of individual Martian lava flows.

2. Geologic Context of SHARAD Data

[4] SHARAD operates at 20 MHz with a 10 MHz bandwidth, and it has a free-space vertical resolution of 15 m [*Seu et al.*, 2004], which corresponds to a 5- to 10-m vertical resolution in common geologic materials. The spatial resolution of SHARAD is 3 to 6 km depending on surface roughness, reducible to 0.75 to 1 km in the along-track direction with synthetic aperture focusing [*Seu et al.*, 2004, 2007].

[5] In the plains northwest of Ascraeus Mons, SHARAD detects late time-delay echoes associated with the distal parts of smooth flows (Figure 1). This region has a low

[1]Center for Earth and Planetary Studies, Smithsonian Institution, Washington, D. C., USA.
[2]Institute for Geophysics, University of Texas at Austin, Austin, Texas, USA.
[3]Southwest Research Institute, Boulder, Colorado, USA.
[4]Consortium for Research on Advanced Remote Sensing Systems, Naples, Italy.
[5]INFOCOM Department, Sapienza University of Rome, Rome, Italy.
[6]U.S. Geological Survey, Flagstaff, Arizona, USA.

0094-8276/09/2009GL041234$05.00

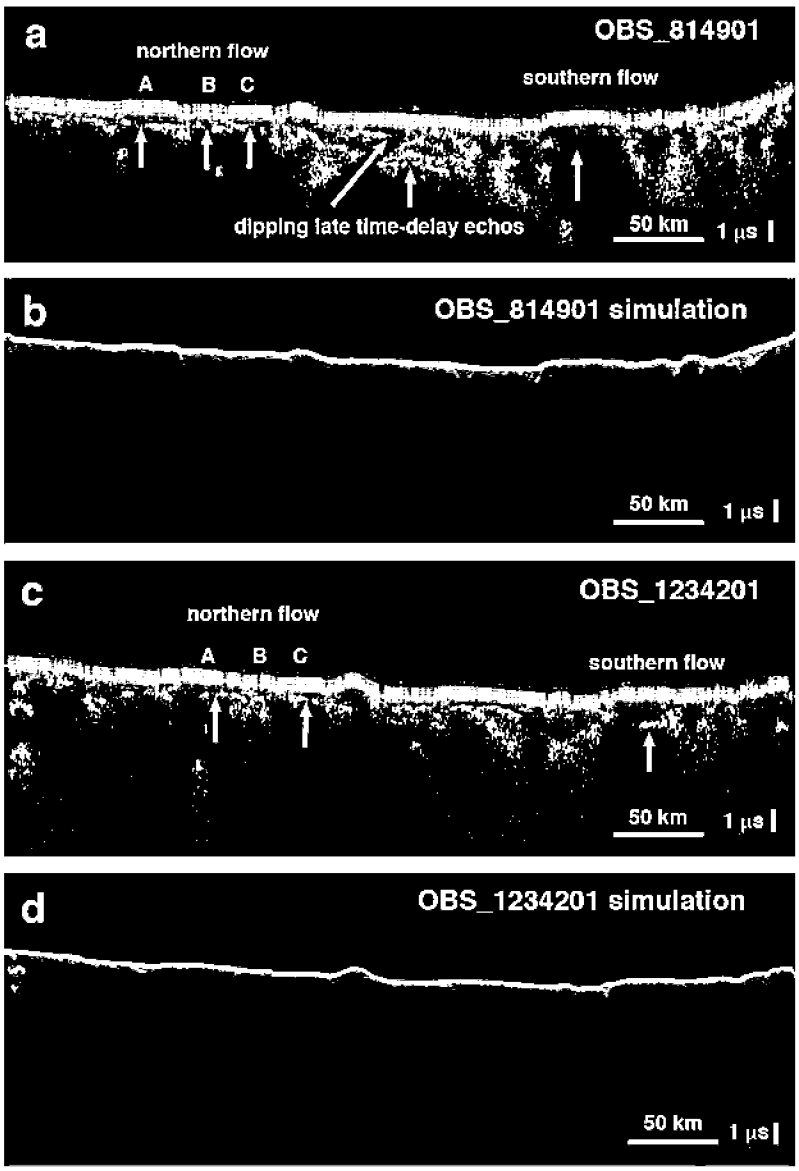

Figure 1. (a and c) Focused radargrams showing interfaces beneath flows west of Ascraeus Mons and (b and d) corresponding clutter simulations. The orbit tracks run from north on the left to south on the right. The location of the orbit tracks is shown in Figure 2. Interfaces are seen beneath both the northern and southern flows. The northern flow has three distinct units, marked A through C. Late time-delay echoes are seen from other locations within the radargrams, but these do not correspond to flows visible on the surface, and may be echoes from dipping reflectors below the surface.

elevation relative to its surroundings and is covered by multiple flow complexes. Most of the lava flows were fed from vents located along the rift zone linking Ascraeus Mons and Pavonis Mons. These flows travel for hundreds of kilometers, and have been interpreted as late-stage flows from rift-zone fissures [*Baloga et al.*, 2003]. The flow thickness varies, but they are typically between 30 and 70 m thick, as measured from Mars Orbiter Laser Altimeter (MOLA) data. Physical models suggest that they may have been emplaced as individual thick flows traveling over flat, smooth surfaces [*Baloga et al.*, 2003]. Models also show that Tharsis-area lavas, including flows from the Ascraeus and Pavonis rift zone, had viscosities consistent with basaltic compositions [*Glaze et al.*, 2009]. These flows were likely emplaced over long time periods, ranging from 1–10 years; flows west of Ascraeus Mons have effusion rates <1000 m^3 s^{-1} which are within the rates of historical terrestrial long-duration eruptions [*Glaze et al.*, 2009]. The long, leveed flows on Mars, including those where SHARAD detects the subsurface, may therefore be similar to many terrestrial basaltic flows [*Glaze et al.*, 2009; *Baloga and Glaze*, 2008; *Glaze and Baloga*, 2006].

[6] SHARAD is sensitive to wavelength-scale topographic features that contribute off-nadir surface clutter to the received echoes. However, such echoes are not present in surface clutter simulations performed using a facet-based, geometrical optics radar model incorporating both diffuse and specular scattering [*Holt et al.*, 2006] applied to SHARAD using MOLA-derived surface topography (Figures 1b and 1d). There are also no obvious sources of

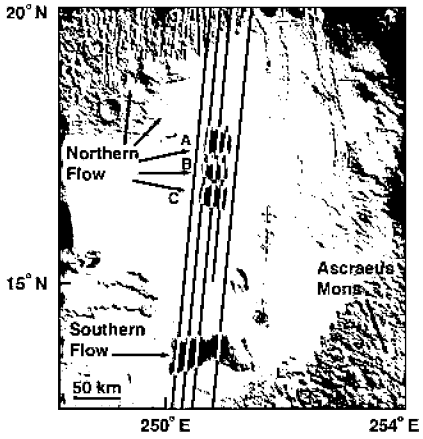

Figure 2. The locations of SHARAD data tracks used for dielectric constant measurements are shown on shaded relief MOLA topography. White bands on the orbit tracks mark the location of subsurface interfaces. The northern and southern flows are marked on the image, and the A, B, and C units of the northern flow complex are shown with arrows. From left to right, the orbit track observation numbers are: 423301, 1234201, 814901, 189901, and 1078601.

clutter in available imaging data of the region at locations required to produce the observed post-nadir echoes. We therefore interpret the late-time delay echoes as interfaces between the flows and the underlying terrain. Consistency of echoes across multiple tracks further reinforces this interpretation.

[7] SHARAD data (Figures 1a and 1c) are typically shown as radargrams, with time-delay increasing down the y-axis and along-track distance increasing along the x-axis. The radargrams used in this study were processed using a synthetic aperture focusing algorithm, and no ionospheric corrections were performed because the data were collected at night. Radargrams in our study area (Figure 1) show that SHARAD penetrates through these flows in two distinct areas: in the northern part of the basin, where a flow complex originates south of Alba Patera, and in the southern part, where the flows originate at the Ascraeus-Pavonis rift (Figure 2). The entire basin is covered in dust, and wind streaks are common. Figure 3 is a HiRISE image of a portion of the northern flows that illustrates the smooth, flat and dust-covered surface. In 12.6-cm wavelength ground-based radar images, the northern flow has fairly low backscatter values, while the southern flow is moderately bright [*Harmon and Nolan*, 2007]. This suggests that there may be a variable dust covering in the area, and that beneath the dust layer, the flows have a high permittivity or a rough surface texture.

[8] There are some differences in morphology between the northern and southern flows. The northern flow complex is thinner and transforms from a channelized flow into broad sheets that spread out laterally into the basin. The SHARAD orbit tracks cross three of these sheets, labeled A, B, and C in Figures 1 and 2. The southern flow is thicker, has well-defined distal lobes, and a central channel. SHARAD only detects subsurface interfaces beneath the thinnest parts of these distal lobes.

[9] The radargrams in Figure 1 show other late-time delay features that are not present in clutter simulations (Figures 1b and 1d) and that do not match the positions of surface flows. In cases with well-defined dipping features, there may be an interface beneath the flat basin surface, perhaps similar to the Amazonis plains reflectors [*Campbell et al.*, 2008]. It is also possible that in some cases small clutter sources may be causing the late-time delay features. Since the depth and origin of these features is uncertain, they are not used for the dielectric constant measurements.

3. Measurement of Dielectric Properties

[10] The SHARAD data can be used to measure the complex dielectric constant ($\varepsilon' \pm i\varepsilon''$) of the lava flows. We estimate the permittivity of the flows by comparing the measured time delay of returns from the subsurface with altimetry measurements of the flow heights relative to the surrounding plains. The permittivity (ε') can be computed from:

$$\varepsilon' = \left(\frac{c\Delta t}{2h}\right)^2 \quad (1)$$

where h is the height relative to the surrounding plains as measured from MOLA topography and Δt is the two-way time delay between the surface and subsurface echoes measured from the radargram. The largest source of error in the derivation of the permittivity is a systematic error caused by the unknown depth of the subsurface interface, which is needed to compute h from the MOLA data. For the basin flows described here, the topography changes slowly, and so straight lines were extrapolated from the surrounding terrain to approximate the subsurface interface depth.

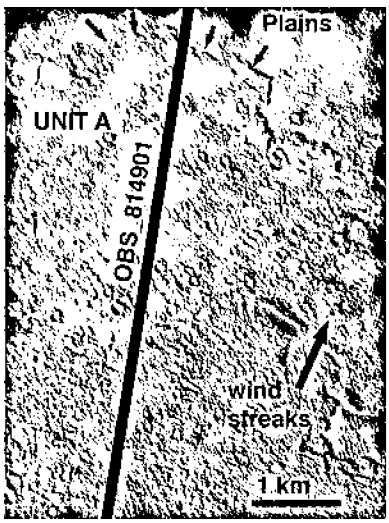

Figure 3. HiRISE image (ESP_012283_1980) of a section of the northern lava-flow complex at 17.69°N and 251.13°E. The SHARAD orbit track (observation 814901) is shown with a black line. The boundary between the plains and "unit A" of the flow is shown by arrows at the top of the image. The surface is flat and dust covered, and wind streaks are common in the area.

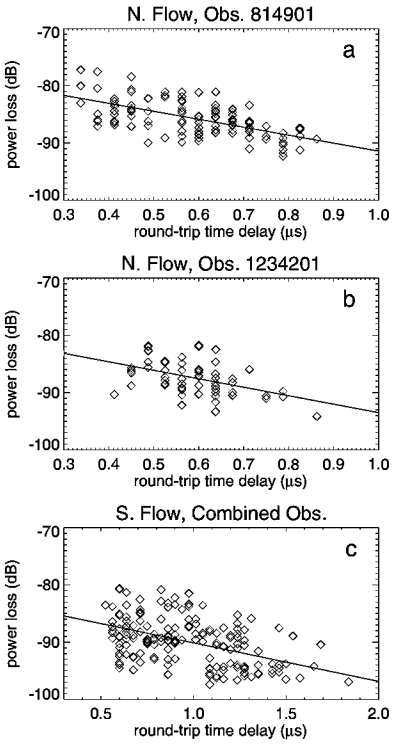

Figure 4. Power versus delay time for the northern and southern flows. (a) Northern flow, observation 814901; (b) northern flow, observation 1234201; (c) southern flow, combined and normalized data from orbit tracks 423301, 814901, 1078601, 1234201. Sloping lines show least-squares fits used for the loss-tangent estimation.

[11] For the northern flow, the permittivity was measured using three orbit tracks that cross the flow. For these tracks, it was assumed that the basal interface is a straight, sloped line that follows the downhill trend of the surrounding terrain. Permittivity values were derived for two segments of the flow in each orbit track. The ε' values range from 6.2 to 17.3, with an average of 12.2 (Table S1 of the auxiliary material).[1] If the basal interface is slightly deeper than assumed, h will be larger, and the computed ε' values will be slightly lower than those given here. A slightly shallower interface (above the level of the surrounding plains) would produce slightly higher permittivity values. Pumice, volcanic ash, and tuff have permittivity values between ~2.5 and 3.5 [*Ulaby et al.*, 1988; *Campbell and Ulrichs*, 1969], while most terrestrial and lunar basalts have ε' values between 7 and 11 [*Carrier et al.*, 1991; *Campbell and Ulrichs*, 1969]. The permittivity values computed for the northern flow are clearly higher than those measured for the Medusae Fossae Formation pyroclastics [*Carter et al.*, 2009], implying a dense rock.

[12] For the southern flow, the permittivity was measured using four orbit tracks. In this case, the plains north of the flow are fairly flat, and so the subsurface interface was assumed to be a continuation of the flat surface to the immediate north of the flow. Here, the computed permittivities range from 7.0 to 14.3 with an average of 9.8 (Table S1). As with the northern flow, if the basal interface is slightly deeper than assumed, the computed ε' values will be lower, and if the interface occurs higher in the column, the ε' values will be higher. For both the northern and southern flows, a low computed permittivity (like that measured for the MFF) is only possible if the flows are sitting on a bench structure, which seems highly unlikely.

[13] For dry materials, the permittivity is primarily influenced by density. Empirical studies have yielded a relationship of:

$$\varepsilon' = 1.96^{\rho} \tag{2}$$

where ρ is the density in g cm^{-3} [*Ulaby et al.*, 1988]. Inverting equation (2) for density, we find values of 3.4 to 3.7 g cm^{-3} from the average measured permittivities. Since basalts commonly have densities greater than 3 g cm^{-3}, whereas most granitic rocks have densities between 2.5 and 3.0 g cm^{-3} [*Johnson and Olhoeft*, 1984], the measured permittivity values for the Martian flows are more consistent with basalt and most likely do not indicate a felsic composition.

[14] In cases where the subsurface interface is visible at a different depths spanning tens of meters, it is also possible to measure the loss tangent (tan δ) of the material. The loss tangent can be written as [*Campbell et al.*, 2008]:

$$\tan\delta = \frac{\varepsilon''}{\varepsilon'} = \sqrt{\left[2*\left(\frac{\lambda}{4\pi c\Delta t}\ln(L)\right)^2+1\right]^2-1} \tag{3}$$

where λ is the SHARAD free-space wavelength of 15 m and L is the power loss per unit of time Δt. This formulation assumes that the surface and subsurface roughness are constant over the measurement area, and that the dielectric contrast at each interface is constant over the measurement area.

[15] In the case of the northern flow, separate fits of power loss versus time delay were made for two orbit tracks. During the standard processing, each orbit track is normalized to the noise background. Subsurface power loss versus time delay with corresponding linear fits are shown in Figures 4a and 4b). Since the northern flow is very flat with a fairly constant echo from the surface, we show the measured power values at each subsurface interface without any normalization to the surface echo. The fits to the two orbit tracks yielded loss-tangent values of 0.025 and 0.027, with a total range (including fitting errors) of ~0.02 to 0.03. Data for the fits are shown in Table S2.

[16] In the case of the southern flow, there is not sufficient change in the subsurface interface depth within each orbit track to get a reliable fit. In order to combine power measurements from multiple tracks, the data were normalized to remove possible effects of changes in antenna gain from one orbit to another due to spacecraft orientation or solar panel position. We show the normalized power for the four orbit tracks plotted together with the best-fit line in Figure 4c. Here, the measured power values for the subsurface interface were divided by the average surface echo over the lava flow surface. This normalization can introduce errors if the surface roughness of the flow is different in

[1] Auxiliary materials are available in the HTML. doi:10.1029/2009GL041234.

each orbit track. However, there is always some potential error involved with changing surface roughness within each track, and the terrain appears very uniform in images. The normalization had the desired effect of removing systematic brightness variations between tracks caused by changes in antenna gain. For the southern flow, the derived loss tangent is 0.012, with a total range, including derived fitting errors, of 0.011 to 0.014 (Table S2).

[17] The measured loss tangents are common values for terrestrial and lunar volcanic rocks, including basalts [*Carrier et al.*, 1991; *Ulaby et al.*, 1988; *Campbell and Ulrichs*, 1969]. They are higher than those derived for the sediment layers in Amazonis [*Campbell et al.*, 2008] and for the Medusae Fossae Formation pyroclastics [*Watters et al.*, 2007]. Loss tangents between 0.01 and 0.03 imply a low to moderate concentration of radar-wave absorbing minerals such as ilmenite or hematite. For example, some lunar basalts with a high fraction of ilmenite (10–15% TiO_2) have loss tangents approaching ~0.1 [*Carrier et al.*, 1991].

4. Conclusions

[18] The lava flows west of Ascraeus Mons have high permittivities and moderate loss tangents that are consistent with high-density lavas such as basalt. Although the flows have a high permittivity, the radar is able to penetrate into the flows, probably because a low-permittivity dust covering allows the incident wave to travel into the subsurface through interfaces with smaller dielectric contrasts (i.e., less impedance mismatch). The loss tangents of the flows are moderate, and the flows therefore do not contain large amounts of radar-wave absorbing minerals.

[19] **Acknowledgments.** We thank the SHARAD Operations Center team, including Emanuele Giacomoni, Federica Russo, Marco Cutigni, Oreste Fuga, Riccardo Mecozzi, Armando Valle, Leonardo Travaglino, and Marco Mastrogiuseppe for their assistance with targeting, calibration, and data processing. The Shallow Subsurface Radar (SHARAD) was provided by the Italian Space Agency through a contract with Thales Alenia Space Italia, and it is operated by the INFOCOM Department, University of Rome "La Sapienza". LMC was supported under NASA Mars Reconnaissance Orbiter Participating Scientist grant NNH06ZDA001N.

References

Baloga, S. M., and L. S. Glaze (2008), A self-replication model for long channelized lava flows on the Mars plains, *J. Geophys. Res.*, *113*, E05003, doi:10.1029/2007JE002954.

Baloga, S. M., P. J. Mouginis-Mark, and L. S. Glaze (2003), Rheology of a long lava flow at Pavonis Mons, Mars, *J. Geophys. Res.*, *108*(E7), 5066, doi:10.1029/2002JE001981.

Campbell, M. J., and J. Ulrichs (1969), Electrical properties of rocks and their significance for lunar radar observations, *J. Geophys. Res.*, *74*, 5867–5881, doi:10.1029/JB074i025p05867.

Campbell, B. A., L. M. Carter, R. J. Phillips, N. E. Putzig, J. J. Plaut, A. Safaeinili, R. Seu, D. Biccari, A. Egan, and R. Orosei (2008), SHARAD radar sounding of the Vastitas Borealis Formation in Amazonis Planitia, *J. Geophys. Res.*, *113*, E12010, doi:10.1029/2008JE003177.

Carrier, W. D., G. R. Ohloeft, and W. Mendell (1991), Physical properties of the lunar surface, in *Lunar Sourcebook*, pp. 457–567, Cambridge Univ. Press, New York.

Carter, L. M., et al. (2009), Shallow radar (SHARAD) sounding observations of the Medusae Fossae Formation, Mars, *Icarus*, *199*, 295–302, doi:10.1016/j.icarus.2008.10.007.

Glaze, L. S., and S. M. Baloga (2006), Rheologic inferences from the levees of lava flows on Mars, *J. Geophys. Res.*, *111*, E09006, doi:10.1029/2005JE002585.

Glaze, L. S., S. M. Baloga, W. B. Garry, S. A. Fagents, and C. Parcheta (2009), A hybrid model for leveed lava flows: Implications for eruption styles on Mars, *J. Geophys. Res.*, *114*, E07001, doi:10.1029/2008JE003278.

Harmon, J. K., and M. C. Nolan (2007), Arecibo radar imaging of Mars during the 2005 opposition, paper presented at the Seventh International Conference on Mars, Lunar Planet. Inst., Pasadena, Calif.

Harmon, J. K., R. E. Arvidson, E. A. Guinness, B. A. Campbell, and M. A. Slade (1999), Mars mapping with delay-Doppler radar, *J. Geophys. Res.*, *104*, 14,065–14,089, doi:10.1029/1998JE900042.

Holt, J. W., M. E. Peters, S. D. Kempf, D. L. Morse, and D. D. Blankenship (2006), Echo source discrimination in single-pass airborne radar sounding data from the Dry Valleys, Antarctica: Implications for orbital sounding of Mars, *J. Geophys. Res.*, *111*, E06S24, doi:10.1029/2005JE002525.

Johnson, G. R., and G. R. Olhoeft (1984), Density of rocks and minerals, in *Handbook of Physical Properties of Rocks*, vol. 3, edited by R. S. Carmichael, pp. 1–38, CRC Press, Boca Raton, Fla.

Seu, R., D. Biccari, R. Orosei, L. V. Lorenzoni, R. J. Phillips, L. Marinangeli, G. Picardi, A. Masdea, and E. Zampolini (2004), SHARAD: The MRO 2005 shallow radar, *Planet. Space Sci.*, *52*, 157–166, doi:10.1016/j.pss.2003.08.024.

Seu, R., et al. (2007), SHARAD sounding radar on the Mars Reconnaissance Orbiter, *J. Geophys. Res.*, *112*, E05S05, doi:10.1029/2006JE002745.

Simpson, R. A., G. L. Tyler, M. Pätzold, and B. Häusler (2007), Inference of electrical and physical surface properties from Mars Express bistatic radar, paper presented at the Seventh International Conference on Mars, Lunar Planet. Inst., Pasadena, Calif.

Ulaby, F. T., T. Bengal, J. East, M. C. Dobson, J. Garvin, and D. Evans (1988), Microwave dielectric spectrum of rocks, *Rep. 23817-1-T*, Univ. of Mich. Radiat. Lab., Ann Arbor.

Watters, T. R., et al. (2007), Radar sounding of the Medusae Fossae Formation Mars: Equatorial ice or dry, low-density deposits?, *Science*, *318*, 1125–1128, doi:10.1126/science.1148112.

B. A. Campbell and L. M. Carter, Center for Earth and Planetary Studies, Smithsonian Institution, P.O. Box 37012, Washington, DC 20013, USA. (carterl@si.edu)

A. F. Egan, R. J. Phillips, and N. E. Putzig, Southwest Research Institute, 1050 Walnut St., Ste. 300, Boulder, CO 80302, USA.

J. W. Holt, Institute for Geophysics, University of Texas at Austin, 4412 Spicewood Springs Rd., Bldg. 600, Austin, TX 78759, USA.

S. Mattei, Consortium for Research on Advanced Remote Sensing Systems, Via J. F. Kennedy 5, I-80125 Naples, Italy.

C. H. Okubo, U.S. Geological Survey, 2255 N. Gemini Dr., Flagstaff, AZ 86001, USA.

R. Seu, INFOCOM Department, Sapienza University of Rome, Via Eudossiana 18, I-00184 Rome, Italy.